Insulator-to-metal transition induced by disorder in a model for manganites

C. Şen, G. Alvarez, and E. Dagotto
National High Magnetic Field Lab and Department of Physics, Florida State University, Tallahassee, Florida 32310, USA
(Received 16 January 2004; published 31 August 2004)

The physics of manganites appears to be dominated by phase competition among ferromagnetic metallic and charge-ordered antiferromagnetic insulating states. Previous investigations [Burgy *et al.*, Phys. Rev. Lett. **87**, 277202 (2001)] have shown that quenched disorder is important to smear the first-order transition between those competing states, and induce nanoscale inhomogeneities that produce the colossal magnetoresistance effect. Recent studies [Motome *et al.*, Phys. Rev. Lett. **91**, 167204 (2003)] have provided further evidence that disorder is crucial in the manganite context, unveiling an unexpected insulator-to-metal transition triggered by disorder in a one-orbital model with cooperative phonons. In this paper, a qualitative explanation for this effect is presented. It is argued that the transition occurs for disorder in the form of local random energies. Acting over an insulating states made out of a checkerboard arrangement of charge, with "effective" site energies positive and negative, this form of disorder can produce lattice sites with an effective energy near zero, favorable for the transport of charge. This explanation is based on Monte Carlo simulations and the study of simplified toy models, calculating the density-of-states, cluster conductances using the Landauer formalism, and other observables. A percolative picture emerges. The applicability of these ideas to real manganites is discussed.

DOI: 10.1103/PhysRevB.70.064428 PACS number(s): 75.47.Lx, 75.30.Mb, 75.30.Kz

I. INTRODUCTION

The study of manganites—the materials with the colossal magnetoresistance—continues attracting the attention of condensed matter experts.[1,2] These compounds are interesting for their potential technological applications as "read sensors" in computers, as well as for the basic science challenges that their unusual properties represent for our understanding of transition-metal oxides. It is widely believed that strong correlations are crucial to understand these manganese oxides, either in the form of large Coulombic interactions or large electron Jahn-Teller phonon couplings, or both simultaneously. Some of their unusual properties include a remarkable response to magnetic fields, with the dc resistivity changing by as much as 10 or more orders of magnitude in some compounds upon the application of fields of order 1 Tesla. Another interesting property is the rich phase diagram that these materials present, with competition of very different states mainly involving ferromagnetic (FM) metallic and charge-ordered (CO) antiferromagnetic (AF) phases. Moreover, in recent years a plethora of experiments have unveiled a remarkable tendency to form inhomogeneities, which occur mainly at the nanoscale but with some investigations reporting domains as large as a submicrometer in size.[3] This spontaneous generation of nanoclusters was predicted theoretically when phase separation tendencies were unveiled in the first Monte Carlo simulations of models for manganites in 1998 by Yunoki *et al.*,[4] then confirmed and refined experimentally in dozens of efforts.[5] The successful cross-fertilization between theory and experiment is remarkable in the area of Mn-oxides, leading to considerable progress in recent years. These studies may have consequences not only for manganites, but for a variety of other compounds where inhomogeneities have been found in experiments, including the famous high-temperature superconductors.[6]

Among the leading candidates to understand the CMR effect is the "phase separation" scenario.[2,5,7] In this context, the state that is believed to be abnormally susceptible to external magnetic fields is made out of coexisting clusters of two competing phases. The clusters involving the FM state have random orientations of their magnetic moments, leading to an overall vanishing magnetization. However, the "building blocks" of the FM state (i.e., the FM nano clusters) are preformed and for this reason the state reacts rapidly to magnetic fields, aligning the nanocluster moments in the presence of small fields. Energetically it is quite different to form a FM state from "scratch," as opposed to having preformed FM islands that only need to reorient their magnetic moments to generate global ferromagnetism. The competing state is also important in the proposed CMR state, since it provides walls that prevent the alignment of the nanoclusters in the absence of external fields.[5,7]

In order to stabilize this type of CMR states, the role of quenched disorder appears to be important.[7] This disorder prevents the system from being totally ferromagnetic or totally CO-AF, as it occurs in the clean limit where a first-order phase transition separates the states.[2,5] Small amounts of quenched disorder locally favor one phase over the other, leading to the inhomogeneous patterns found in simulations, which are believed to correspond to those in experiments. These predictions were beautifully confirmed by the group of Tokura,[8] by means of a careful study of a particular Mn-oxide that spontaneously forms a structure very close to the clean limit, since all ions order in a regular pattern. This compound presents a "bicritical" phase diagram, with a first-order FM-AF transition in excellent agreement with Monte Carlo simulations.[9] When the material is rapidly quenched in the growing process, such that the disorder is now incorporated in the distribution of trivalent ions, then a behavior characteristic of many other manganites is recovered. In particular, a large CMR is found in the presence of disorder, a result compatible with the theoretical predictions.[5,7] Recent investigations by Sato, Lynn, and Dabrowski[10] arrived to

similar conclusions studying $La_{0.54}Ba_{0.46}MnO_3$. Other recent investigations[11] have shown that the addition of lattice elastic effects (due to the cooperative nature of the Jahn-Teller distortions) makes the disorder strength needed to induce the CMR phenomenon smaller in magnitude than without elasticity, and avoids limitations in the critical dimension that the naive use of Imry-Ma argumentations[12] would suggest. The relevance of elastic effects has been remarked extensively in recent literature as well.[13] Other power-law decaying effects, such as unscreened Coulomb interactions, have also been proposed as relevant in this context.[14] In addition, investigations of a variety of models of percolation have shown that "correlated" disorder—to mimic elastic effects—can even change the order of the transition rendering it first order.[15] It may occur that "infinitesimal" disorder is enough to trigger and stabilize a phase separation process that is intrinsic to systems with first-order phase transitions. Nevertheless, in practice at least small amounts of disorder appear to be crucial to produce the inhomogeneous state that theorists proposed as the key factor to understand the CMR physics.

More recent investigations by Motome, Furukawa, and Nagaosa[16] have provided important information for the theoretical understanding of manganese oxides. Monte Carlo simulations of the one-orbital double-exchange model including cooperative phonons have revealed an interesting transition from an insulator to a metal upon the introduction of quenched disorder into a CO state. The disorder is in the form of on-site random energies. Once again, the key role of disorder is unveiled by these simulations. Independently, Aliaga *et al.*[9] arrived at similar conclusions studying a two-orbital model for manganites including cooperative Jahn-Teller phonons. These authors noticed that disorder drastically affects the CE charge-ordered state, transforming it into a "CE glass." Overall, it is clear that the use of cooperative phonons (for previous work see Refs. 17 and 18 and references therein), as opposed to the simpler case of noncooperative lattice distortions, is important to unveil interesting effects of manganite models, that may be of relevance to experiments.

It is our purpose in this work to provide an intuitive understanding of the results of Ref. 16, mainly addressing the transition from an insulator to a metal upon the introduction of disorder, a result which seems counter-intuitive at first sight. Here, it is argued that the transition occurs through an interesting *percolative-like* process due to the effect of random on-site energies over a charge-ordered state. The sites of the lattice that had an effective "negative energy" in the CO state—namely those that were populated with localized electrons in the checkerboard arrangement—may acquire a nearly zero total energy due to the influence of that type of disorder. The "nearly zero energy" sites can contribute to form a metallic state which is highly inhomogeneous in instantaneous Monte Carlo snapshots, although it slowly evolves with time (dynamical) as the Monte Carlo simulation progresses. It is concluded that the case found in Refs. 9 and 16 provides another very interesting example where a combination of explicit quenched disorder and charge-ordering tendencies leads to nontrivial physics, including insulator-metal transitions. The main merit of the present manuscript is to clarify the key role of disorder in a very simple model, with easy-to-understand qualitative argumentations. This adds extra support to the idea that quenched disorder is crucial in CMR manganites.

The organization of the paper is as follows. In Sec. II, the model with cooperative phonons and disorder is discussed. The main results of the Monte Carlo analysis are in Sec. III, including the phase diagram, density-of-states with and without disorder, and the calculation of conductances. A simplified model that captures the essence of the main model is introduced in Sec. IV. Both models behave very similarly. Our proposed explanation of the insulator-metal transition is presented in Sec. V, where the inhomogeneous nature of the metallic state is described. Simulations with random hoppings and by freezing the localized spins are also reported in this section. Conclusions are presented in Sec. VI.

II. MODEL

The Hamiltonian used in this study contains Mn e_g itinerant electrons coupled to the t_{2g} Mn core-spins, and also to phonons according to[18]

$$H = -t\sum_{\langle \mathbf{i},\mathbf{j}\rangle,\sigma}(c^{\dagger}_{\mathbf{i}\sigma}c_{\mathbf{j}\sigma}+\text{h.c.}) - 2J_{\text{H}}\sum_{\mathbf{i}}\mathbf{s}_{\mathbf{i}}\cdot\mathbf{S}_{\mathbf{i}} - \lambda t\sum_{\mathbf{i},\alpha,\sigma}(u_{\mathbf{i},-\alpha}-u_{\mathbf{i},\alpha})c^{\dagger}_{\mathbf{i}\sigma}c_{\mathbf{i}\sigma}. \quad (1)$$

Here, the first term represents the kinetic energy of the carriers hopping between Mn atoms on a d-dimensional cubic lattice, with t the hopping amplitude for the process. $\langle \mathbf{i},\mathbf{j}\rangle$ denotes nearest-neighbor pairs of sites, and the rest of the notation is standard. The second term is the Hund interaction between itinerant $\mathbf{s}_{\mathbf{i}}$ and localized $\mathbf{S}_{\mathbf{i}}$ spins, with J_{H} the Hund coupling constant. The third term describes the energy corresponding to the lattice-carrier interaction, with λ denoting the electron-phonon coupling. The appropriate redefinitions of variables allow us to have the energy unit t explicitly in this term (see Ref. 18). The distortions of the six oxygens surrounding Mn at site $\mathbf{i}$ are given by the classical numbers $u_{\mathbf{i},\pm\alpha}$, where in 3D (2D) α runs over three (two) directions x, y, and z (x,y). Quantum phonons are much harder to study numerically, and their analysis is postponed to future publications. One widely-used simplification to the above Hamiltonian, without losing essential physics, is to take the limit $J_{\text{H}}=\infty$, since in manganese oxides the Hund interaction is experimentally known to be large. In this limit, the e_g-electron spin perfectly aligns along the t_{2g}-spin direction. This allows us to reduce the first two terms of the double exchange Hamiltonian to[5]

$$H_{\text{DE}} = -\sum_{\langle \mathbf{i},\mathbf{j}\rangle}[\mathcal{T}(\mathbf{S}_{\mathbf{i}},\mathbf{S}_{\mathbf{j}})d^{\dagger}_{\mathbf{i}}d_{\mathbf{j}}+\text{h.c.}], \quad (2)$$

where

$$\mathcal{T}(\mathbf{S}_{\mathbf{i}},\mathbf{S}_{\mathbf{j}}) = -t\left[\cos\frac{\theta_{\mathbf{i}}}{2}\cos\frac{\theta_{\mathbf{j}}}{2}+\sin\frac{\theta_{\mathbf{i}}}{2}\sin\frac{\theta_{\mathbf{j}}}{2}e^{i(\phi_{\mathbf{i}}-\phi_{\mathbf{j}})}\right]. \quad (3)$$

$\theta_{\mathbf{i}}$ and $\phi_{\mathbf{i}}$ are the spherical coordinates of the core spin $\mathbf{S}_{\mathbf{i}}$ at site $\mathbf{i}$. The new operators $d^{\dagger}_{\mathbf{i}}$ create an electron at site $\mathbf{i}$ with

spin parallel to the core spin at **i**. Within this large Hund-coupling approximation, the third term that produces lattice distortions becomes

$$H_{\text{e-ph}} = -\lambda t \sum_{\mathbf{i},\alpha} (u_{\mathbf{i},-\alpha} - u_{\mathbf{i},\alpha}) d_{\mathbf{i}}^{\dagger} d_{\mathbf{i}}. \tag{4}$$

This tendency is balanced by an opposite crystal elastic energy that represents the stiffness of the Mn-O bonds:

$$H_{\text{ph}} = t \sum_{\mathbf{i},\alpha} (u_{\mathbf{i},\alpha})^2. \tag{5}$$

In the present investigations, it is important to also consider a disorder term of the form

$$H_{\Delta} = \sum_{\mathbf{i}} \Delta_{\mathbf{i}} n_{\mathbf{i}}, \tag{6}$$

where $\Delta_{\mathbf{i}}$ is chosen randomly from some distribution (box, bimodal, Gaussian) and $n_{\mathbf{i}} = d_{\mathbf{i}}^{\dagger} d_{\mathbf{i}}$. Hence, the full Hamiltonian used in the present study is given by

$$H = H_{\text{DE}} + H_{\text{e-ph}} + H_{\text{ph}} + H_{\Delta}. \tag{7}$$

In this paper, we have considered two types of disorder: (i) a binary or bimodal distribution where $\Delta_{\mathbf{i}} = \pm\Delta$, with Δ being a constant, and (ii) a box distribution where Δ can take any value in some interval $[-\Delta', \Delta']$. In order to compare the results between these two distributions, one should establish a relation among them. This can be done by requiring that the standard deviation Δx should be the same for both. Since $\langle x \rangle = 0$, one has

$$(\Delta x)^2 = \langle x^2 \rangle = \int_{-\infty}^{\infty} dx x^2 P(x), \tag{8}$$

where $P(x) = \delta(x+\Delta) + \delta(x-\Delta)$ for the binary distribution and $P(x) = 1$ in the interval $x \in [-\Delta', \Delta']$ for the box distribution. This gives $\langle x^2 \rangle = 2\Delta^2$ for the former, and $\langle x^2 \rangle = 2\Delta'^3/3$ for the latter. Hence, the relation between Δ and Δ' should be $\Delta' = (3\Delta^2)^{1/3}$.

The model used in this paper contains only one orbital in the e_g sector, instead of the more realistic case of two active orbitals. Since using two orbitals increases substantially the CPU time, in this first analysis the focus is on the one-orbital situation. Also note that Motome and collaborators have studied a similar model,[16] as remarked in the Introduction, but they implemented the cooperative effect between oxygens (namely the effect by which a given oxygen is shared by two octahedra) in a different manner. This does not represent a problem since our results for the phase diagram and density-of-states are very similar to those of Ref. 16. Finally, the technique to be used involves the exact diagonalization of the fermionic sector, while for the classical degrees of freedom, a standard Metropolis is used. Additional details of the numerical methods are not presented here since they have been extensively discussed in previous literature.[2,5]

III. INSULATOR-TO-METAL TRANSITION INDUCED BY QUENCHED DISORDER

A. Phase diagram

The phase diagram of the model discussed in the previous section was investigated using spin-spin and density-density real-space correlation functions, as well as spin and charge structure functions in **q**-space, which are defined, respectively, as follows:

$$S(\mathbf{x}) = \frac{1}{N} \sum_{\mathbf{i}} \langle \mathbf{S}_{\mathbf{i}} \cdot \mathbf{S}_{\mathbf{i}+\mathbf{x}} \rangle, \tag{9}$$

$$n(\mathbf{x}) = \sum_{\mathbf{i}} \langle n_{\mathbf{i}} \rangle \langle n_{\mathbf{i}+\mathbf{x}} \rangle - \frac{1}{N} \left(\sum_{\mathbf{i}} \langle n_{\mathbf{i}} \rangle \right)^2, \tag{10}$$

$$S(\mathbf{q}) = \sum_{\mathbf{i},\mathbf{j}} \langle \mathbf{S}_{\mathbf{i}} \cdot \mathbf{S}_{\mathbf{j}} \rangle e^{i\mathbf{q}\cdot(\mathbf{r}_{\mathbf{i}} - \mathbf{r}_{\mathbf{j}})}, \tag{11}$$

$$n(\mathbf{q}) = \sum_{\mathbf{i},\mathbf{j}} \langle n_{\mathbf{i}} \rangle \langle n_{\mathbf{j}} \rangle e^{i\mathbf{q}\cdot(\mathbf{r}_{\mathbf{i}} - \mathbf{r}_{\mathbf{j}})}. \tag{12}$$

In all of the correlations, $\langle \mathcal{O} \rangle$ stands for the thermal average of the operator $\mathcal{O}$ and is defined by

$$\langle \mathcal{O} \rangle = \frac{\text{Tr}[\mathcal{O} e^{-\beta H}]}{\text{Tr}[e^{-\beta H}]}, \tag{13}$$

where β is the inverse temperature, N is the total number of sites, and the rest of the notation is standard.[19] In the following sections, results are given in units of t, unless otherwise stated. In addition, all the results shown in this manuscript correspond to the case of half-filling $n = 0.5$, where on average there is one electron for every two sites. This was the electronic density studied in Refs. 9 and 16, and typically such density is easily analyzed numerically (contrary to other cases where more complicated charge patterns occur, requiring larger lattices). Moreover, many real manganites have $n = 0.5$.

As a criterion to decide whether a particular ordered phase is stable, namely whether long-range order is present, the equal-time spin and charge correlation functions were used. More specifically, a charge-ordered (CO) phase is here defined as stable if (i) the real-space charge correlation $n(\mathbf{x})$ at the maximum distance possible in the finite-size clusters studied is at least 5% of the maximum value found at distance zero $n(0)$. The 5% criterion is certainly arbitrary, nevertheless it is qualitatively representative of the physics under investigation here. Other criteria, i.e. 10% or 1%, simply lead to phase diagrams slightly shifted up or down in temperature. In addition, (ii) max $n(\mathbf{q})$ must have its maximum value at $\mathbf{q} = (\pi, \pi)$, for a checkerboard charge-ordered state to be defined as stable. These two criteria give very similar results in practice. For the ferromagnetic (FM) phase, a similar definition was used: in this case a FM phase is said to exist when $S(\mathbf{x})$ at the maximum distance is larger than 1% of $S(0)$, which is already normalized to one. In addition, the spin correlation in momentum space must have a robust peak at (0,0). The excellent agreement found here with previous

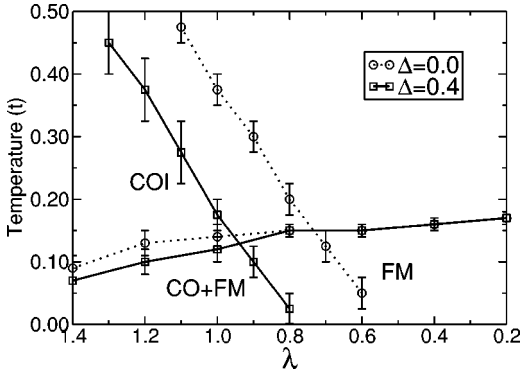

FIG. 1. Monte Carlo phase diagram of the $J_H=\infty$ one-orbital model as given by the Hamiltonian in Eq. (7), for an 8×8 lattice, and overall density $n=0.5$. Results at the values of disorder indicated are shown. The error bars are representative of the different critical temperatures obtained using different starting configurations, as discussed in the text. The number of quenched disorder configurations used for the averages varies from point to point, but the smoothness of the results indicates that there is no crucial dependence with that number.

investigations[9,16] leads us to believe that our criteria for the determination of the phase diagram is robust, and variations around this criteria will not change qualitatively the main conclusions.

In the actual Monte Carlo simulations, the spin and phononic configurations, both assumed to be classical degrees of freedom, are updated according to the Metropolis algorithm. For the 8×8 lattice, the number of Monte Carlo sweeps per site is taken as 10^4 for thermalization, typically followed by another 10^4 sweeps or more for measurements. The simulations were done in a two-fold way. In the first case, the starting configuration of classical spins and oxygen coordinates was chosen to be random, namely a high temperature configuration is selected, followed by a slow cooling down. In the second case, simulations started with an ordered stated at low temperatures, which is followed by a slow heating up. It was observed that both procedures gave fairly consistent results, and the fluctuations in the values of critical temperatures are contained in the error bars shown.

Using the criteria outlined in the previous paragraphs, the phase diagram of model Eq. (7) is shown in Fig. 1. In the clean limit, two phases compete: a charge-ordered phase with a checkerboard arrangement of charge (to be expected in the large λ limit), and a ferromagnetic phase at small λ which is caused by the double exchange mechanism.[2] The existence of these phases and shape of the phase diagram is in excellent agreement with the results of Ref. 16 (see also Refs. 9 and 18) although different criteria to define long-range order were used, independent programs were written, and even the actual models differ in the form in which cooperation is introduced. In the clean limit there is a region where both orders coexist at low temperature, leading to tetracritical behavior. Other investigations of alternative models for manganites produced first-order transitions between competing phases with AF and FM characteristics.[5,9,11] In the present analysis, an AF state is not present and phase competition is probably not so intense as in more realistic cases.

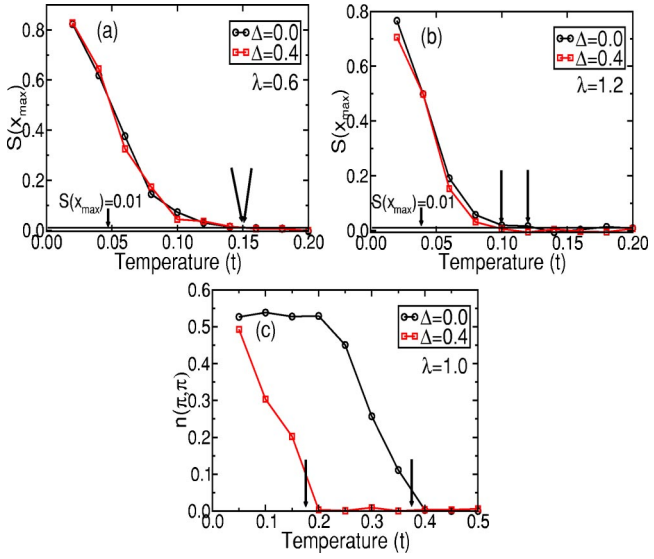

FIG. 2. (Color online) The criteria used for the determination of the Curie temperature T_c: spin-spin correlation function at maximum distance for the cluster studied vs temperature, for $\lambda=0.6$ (a) and $\lambda=1.2$ (b). The $S(x_{max})=0.01$ line is 1% of its maximum value, the criteria used here to determine FM critical temperatures (indicated by the arrows). For T_{CO}, $n(\pi,\pi)$ vs temperature for $\lambda=1.0$ is shown in (c), for two strengths of disorder Δ, and the approximate critical temperatures of the CO-state are indicated. The figures show results for one disorder configuration.

The most interesting results arise upon the introduction of disorder in the form of random local energies. In this case, it was observed that the FM correlations are not much affected by disorder, but the charge correlations are drastically modified. At λ in the range 0.6 to 0.8 and low temperatures, a CO state in the clean limit becomes a charge-disordered state for nonzero Δ (strength of the on-site disorder). This is suggestive of an insulator to metal transition. The phase diagram and prediction of insulator to metal transition based on the study of the density-of-states was previously discussed in Ref. 16 (see also Ref. 9) and our investigations confirm their results. In addition, studies of conductances discussed in the rest of the paper confirm the prediction of an insulator to metal transition triggered by disorder. It is interesting to remark that the FM state does not seem to play any important role in this study, it is the insulating CO-state that is highly susceptible to the introduction of disorder. Thus, the actual competition at the heart of the phenomenon discussed here appears to be among charge-ordered and charge-disordered states, as explained more extensively in the discussion below using a model where the spin degree-of-freedom is removed.

Figure 2 illustrates some of the evidence gathered for the construction of the phase diagram, Fig. 1. In parts (a) and (b) the spin correlations are shown, at two different values of λ, as indicated. In both cases, the behavior of the spin correlations is quite similar before and after disorder is introduced. It appears that this degree of freedom is not crucial for an understanding of the phenomena, since it barely changes with disorder. More relevant is the study of charge ordering, since its associated critical temperature T_{CO} is substantially modified at nonzero Δ. One typical example is shown in Fig.

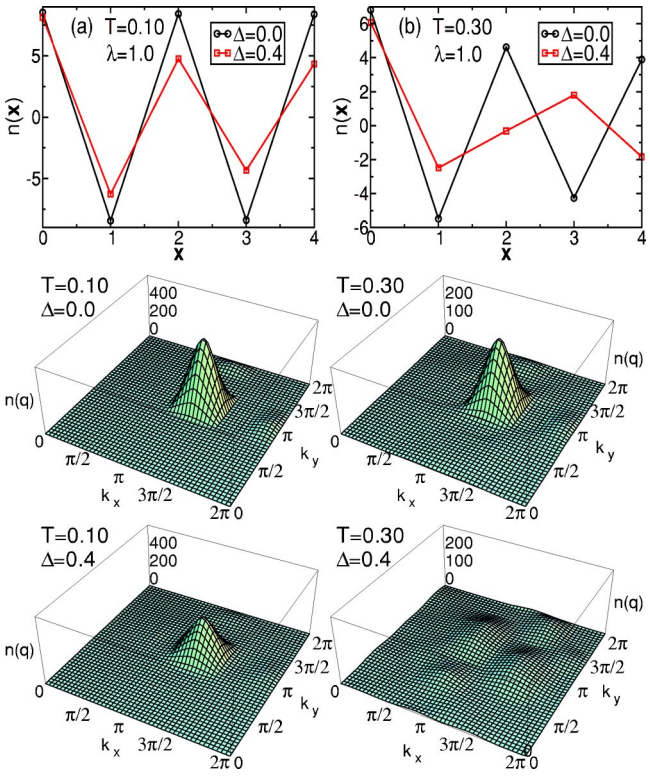

FIG. 3. (Color online) Breakdown of the charge-ordered state with disorder: For small temperatures, $T=0.10$, the CO phase survives the disorder [(a), (c), and (e)]. However, at larger temperatures, $T=0.30$, the initial CO state melts with disorder [(b), (d), and (f)].

2(c): here the charge structure factor at wavevector (π,π) is shown. There is a clear difference between the cases with and without disorder, with a reduction of the critical temperature by roughly a factor two. With hindsight based on the discussion that is presented in the next section, it is understandable that on-site random energies will affect severely a CO state. If these random energies are negative at some of the sites that were not originally populated in the CO state, likely a transfer of charge to those sites will be induced. The reciprocal occurs with positive random energies in sites that were populated in the clean limit. Thus, the phenomenon presented here is expected to be basically related to charge ordering (not spin) and also to depend on the particular form of quenched disorder used, as confirmed later in the discussion.

For completeness, results for just one quenched-disorder configuration of random energies are shown in Fig. 3. Part (a) corresponds to a temperature where both with and without the disorder (strength indicated), a CO state is stabilized. The charge staggered pattern is robust, even with disorder incorporated. This is caused by the cooperative nature of the lattice distortions. On the other hand, at $T=0.30$ [part (b)] the charge staggered pattern is substantially distorted with disorder. This fact is also very clearly shown in the charge structure factor [part (c)] where a robust (π,π) peak is replaced by a fairly featureless background at $T=0.30$ and $\Delta=0.4$. For each individual configuration of disorder, the charge appears

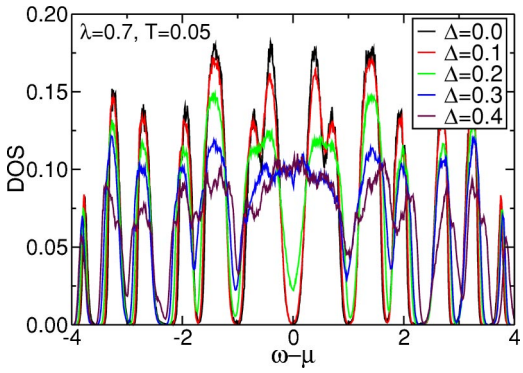

FIG. 4. (Color online) Density-of-states obtained with Monte Carlo simulations at the values of λ and temperature indicated. The lattice is 8×8 in size, and averages over five disorder configurations are presented (the disorder was generated with a bimodal distribution in this example). 10^4 thermalization steps were used, with 10^4 measurements. Values of Δ are indicated. Similar results were also obtained using 4×4 clusters (not shown).

to order following a complicated pattern (b). However, the average over disorder produces a featureless state.

B. Density-of-states

In addition to the equal-time correlations used in the previous section to establish the phase diagram, in this effort the density-of-states (DOS) was also calculated. The procedure to calculate dynamical quantities involves the full diagonalization of the electronic problem for each configuration of classical spins and phonons. Details can be found in Ref. 2.

Interesting results are shown in Fig. 4, illustrating one of the main conclusions of the present investigation, and confirming the predictions of Ref. 16. As expected, the clean-limit case $\Delta=0$ presents a DOS which has a *gap* at the chemical potential, in agreement with the results of Fig. 1 that locate $\lambda=0.7$ and low temperature within the CO phase. The presence of oscillations at nonzero values of ω-μ is due to well-known finite-size effects: a relatively small cluster with periodic boundary conditions typically has a shell structure in their ladder of states. These spurious oscillations do not affect the conclusions of our study. The main result related with Fig. 4 is the interesting dependence of the DOS with the magnitude of Δ. In fact, at $\Delta=0.3$ and higher the original CO gap at the chemical potential has simply vanished, suggesting the instability of the insulating CO-state toward a novel state (presumably metallic) induced by quenched disorder. Understanding the origin of this unexpected insulator-to-metal transition, triggered by disorder, will occupy most of the rest of the present paper.

To convince the reader that the apparently small number of disorder realization used in Fig. 4 is sufficient for our purposes, in Fig. 5 results for five independent quenched-disorder configurations are shown. Qualitatively, the five present states at the chemical potential as observed in the average Fig. 4. To analyze the dependence of the results with the type of disorder introduced, in Fig. 6 results for a box distribution, instead of bimodal, are shown at the couplings indicated. Once again, the DOS presents a CO state at small

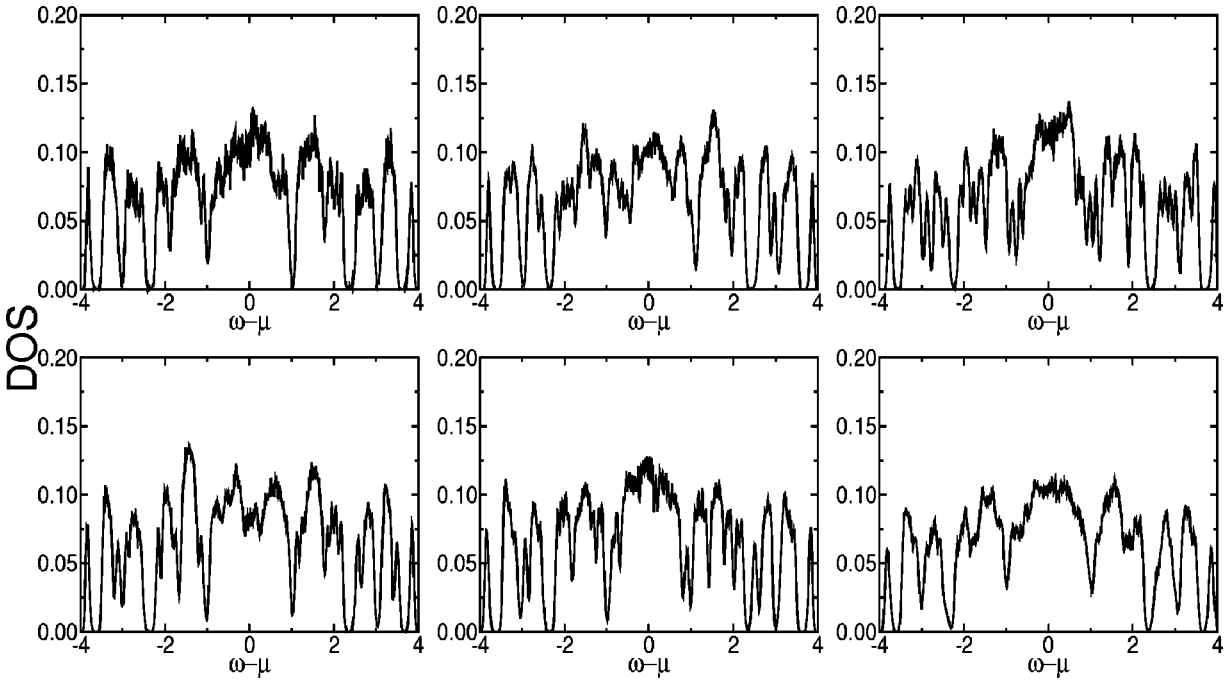

FIG. 5. The first five figures correspond to the DOS obtained with five different quenched-disorder configurations, at the same λ, lattice size, and temperature used in Fig. 4. A bimodal distribution of disorder was employed and results for $\Delta = 0.4$ are shown. All five results are qualitatively similar. The last figure is the average over all five.

Δ, which is replaced by a metallic-like DOS when Δ is increased. To study the dependence of the results with Δ over a wider range, in Fig. 7 results for Δ as large as 1.6 are shown, using a bimodal distribution. At large Δ, it is natural to expect that the states at the Fermi level will not be filled, since this strong disorder *must* induce localization of charge at the sites where the on-site random energy happens to be large and negative. Then, the DOS presents an interesting nonmonotonic behavior with an insulator at both Δ small and large, while the system is metallic at intermediate Δ.

The situation is different for the box distribution. In this case, it is expected that large Δ will not alter the results so dramatically as for the case of the bimodal distribution, since there are always random energies that will happen to be small and they do not lead to localization. This is confirmed by the results of the simulation in Fig. 8, showing that states are present at the Fermi level even for large disorder.

C. Landauer conductance

While the presence of weight at the Fermi level in the DOS is suggestive of a metallic state, it may occur that those states are not extended but localized. To clarify this issue the conductance, G, of clusters described by the Hamiltonians used in this effort was also evaluated. The calculation was carried out using the Kubo formula adapted to geometries usually employed in the context of mesoscopic systems.[20] The actual expression for G is

$$G = 2\frac{e^2}{h}\mathrm{Tr}[(i\hbar\hat{v}_x)\mathrm{Im}\,\hat{\mathcal{G}}(E_\mathrm{F})(i\hbar\hat{v}_x)\mathrm{Im}\,\hat{\mathcal{G}}(E_\mathrm{F})], \qquad (14)$$

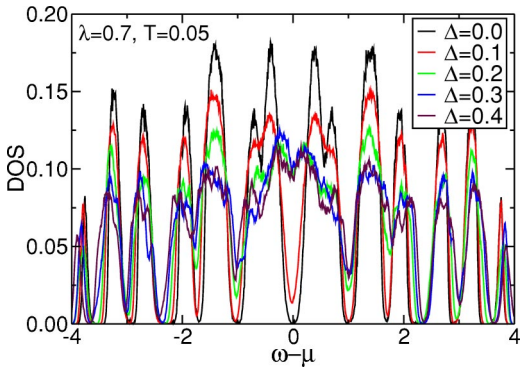

FIG. 6. (Color online) Density-of-states (averaged over five disorder configurations) using a box distribution (instead of bimodal). 10^4 thermalization steps were used, with 10^4 sweeps for measurements.

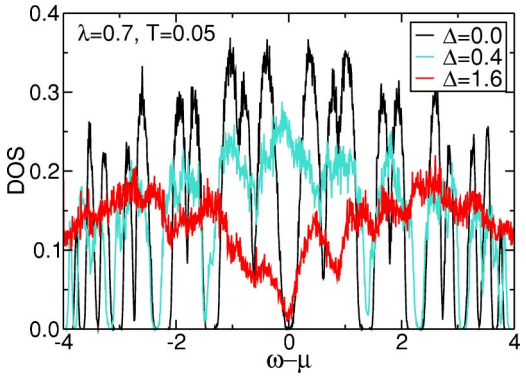

FIG. 7. (Color online) The "closing" and "re-opening" of the gap in the density-of-states as the disorder strength Δ is increased, using a bimodal distribution. Temperature, λ, and Δ's are indicated.

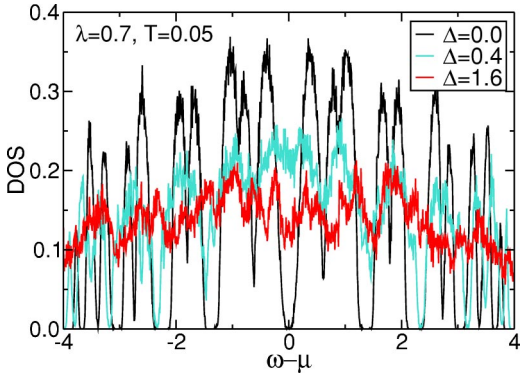

FIG. 8. (Color online) Analog of Fig. 7 but for a box distribution. In this case, the gap that closes at intermediate Δ does not form again for larger values of the disorder strength.

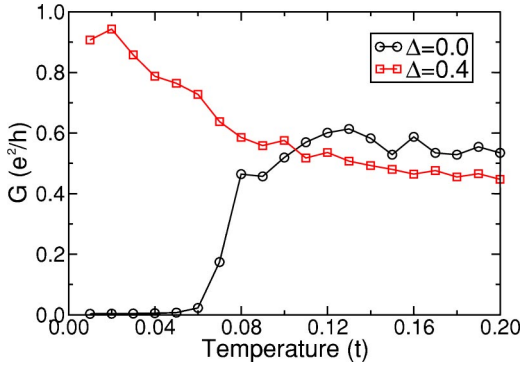

FIG. 10. (Color online) Conductance (e^2/h) vs temperature for the one-orbital model with cooperative phonons at $\lambda=0.7$ and using a 12×12 cluster, in the geometry shown in Fig. 9.

where $\hat{v}_x$ is the velocity operator in the x direction (assuming current flows along that direction) and Im $\hat{\mathcal{G}}(E_F)$ is obtained from the advanced and retarded Green's functions using $2i$ Im $\hat{\mathcal{G}}(E_F)=\hat{\mathcal{G}}^R(E_F)-\hat{\mathcal{G}}^A(E_F)$, where E_F is the Fermi energy. The cluster is considered to be connected by ideal contacts to two semi-infinite ideal leads, as represented in Fig. 9. The current is induced by an infinitesimal voltage drop. This formalism avoids some of the problems associated with finite systems with periodic boundary conditions, such as the fact that the optical conductivity is given by a sum of Dirac δ functions due to the discrete nature of the matrix eigenvalues. Finding a zero-frequency Drude peak with finite weight corresponds, in principle, to an ideal metal—i.e., a system with *zero* resistance—unless an arbitrary width is given to the zero frequency δ-function. In addition, in numerical studies sometimes it occurs that the weights of the zero-frequency delta-peak are *negative* due to subtle finite-size effects.[21] For these reasons, calculations of dc resistivity using finite closed systems are rare in the literature. All these problems are avoided with the formulation described here, which can be readily applied to the Hamiltonians employed in our study where the fermionic sector is quadratic. The problem basically amounts to the calculation of transmissions across nontrivial backgrounds of classical spins and lattice distortions.

In practice, the entire equilibrated cluster, as obtained from the MC simulation, is introduced in the geometry of Fig. 9. The ideal leads enter the formalism through self-energies at the left/right boundaries, as described in Ref. 20. In some cases a variant of the method, explained also in Ref. 20, was used to calculate the conductance: Instead of connecting the cluster to an ideal lead with equal hoppings, a replica of the cluster was used at the sides. This method, although slightly more CPU time consuming, takes into account all of the Monte Carlo data for the cluster, including the periodic boundary conditions. The final step in the calculation is to carry out averages over the localized spin configurations and oxygen coordinates provided by the Monte Carlo procedure. The physical units of the conductance G in the numerical simulations for 2D are e^2/h as can be inferred from Eq. (14). In 2D the conductivity σ coincides with the conductance, while in 3D σ is simply given by the conductance divided by the linear size of the lattice, assumed cubic.

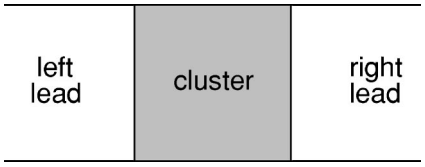

FIG. 9. Geometry used for the calculation of the conductance. The interacting region (cluster) is connected by ideal contacts to semi-infinite ideal leads. The configurations of classical localized spins and phonons are produced by Monte Carlo simulations.

A representative result of our effort is shown in Fig. 10, where G vs temperature is shown at an electron-phonon coupling and disorder strength where the DOS study of the previous section revealed the insulator to metal transition. In the clean-limit, the nearly vanishing value of G at low temperatures reveals the presence of an insulator, which it is known to be a charge-ordered state. The transition to a disordered state occurs with increasing temperature at approximately $T=0.08-0.10$ $(\Delta=0)$, a value compatible but slightly lower than that found through the charge correlations (this may simply be due to the different lattice sizes used). The most remarkable result is shown at $\Delta=0.4$. Here, the conductance is very similar to the clean-limit result at temperatures above the transition, but at low temperatures they are drastically different. Compatible with the finite DOS at the Fermi level found in the previous section, the system with nonzero quenched disorder has a *finite conductance* at low-T, which actually increases with decreasing temperature as in a metallic state. The inverse of the conductance (i.e. the resistivity in 2D) vs T is shown in Fig. 11, using a logarithmic (base 10) scale to amplify the nearly vanishing conductance of the insulating state of Fig. 10. The change of several orders in the resistivity between the clean and dirty limits is in agreement with typical CMR experiments. The introduction of quenched disorder transforms an insulator in the clean limit to a metallic state in the dirty case. As a consequence, the states at the Fermi level induced by disorder that were observed in the previous section indeed correspond to extended states that transport charge, a very interesting result. Note, however, that the conductance in the metallic state is substantially smaller than its maximum value (10 for a 12×12

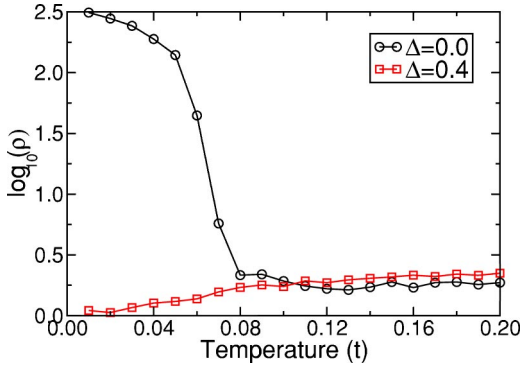

FIG. 11. (Color online) Logarithm (in base 10) of resistivity (inverse of conductivity) vs temperature for the same lattice and couplings used in Fig. 10. Note the similarity of the results with those obtained varying magnetic fields near AF-FM first-order transitions (see Ref. 9).

cluster), indicative of a *dirty metal*. This result is also compatible with experiments in manganites that have revealed similar characteristics.[1,2] Then, the metallic state is far from perfect and there must exist sources of scattering that prevents the smooth flow of charge. In subsequent sections, it will be argued that this metallic state is percolative-like, a result compatible with its relatively high resistance.

In Fig. 12, results for the conductance at low temperature as a function of Δ are shown for two different cluster sizes. The size effects appear to be very small, although the clusters studied are not sufficiently large to show convincingly that a metallic state was indeed stabilized. The behavior as a function of Δ reveals a range of insulating behavior at small Δ, followed by a well-defined peak in the conductance at intermediate values—where Δ is comparable to the gap, as explained later in the text—followed by a subsequent decrease of G at Δ of order 1 or larger. This large-Δ behavior can easily be understood due to strong localization of carriers in that limit. However, the presence of a metallic state at intermediate Δ—as opposed to a smooth interpolation between the two insulating limits at small and large Δ—is puzzling. Its understanding is the main goal of the next section.

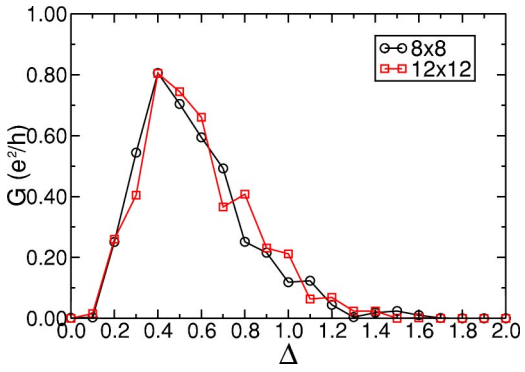

FIG. 12. (Color online) Conductivity vs disorder strength for model Eq. (7), at $\lambda=0.7$ and $T=0.05$. 10,000 thermalization and 2000 measurement Monte Carlo sweeps were used. Results for two lattice sizes are shown, suggesting that finite-size effects could be small.

IV. RESULTS FOR A SIMPLIFIED MODEL

The results presented in the previous section have revealed an insulator to metal transition induced by on-site random-energy disorder, when the clean limit starting state is charge ordered. This conclusion appears clearly both in the DOS and in the conductance, and it is already evident in lattices as small as 4×4. Then, the mechanism must be easy to understand since it cannot depend on subtleties related with the bulk limit or large correlation lengths. In order to clarify the origin of the insulator-metal transition, here a "toy model" involving only electrons will be introduced, and shown to behave quite similarly as the actual "real model" that has electrons, localized spins, as well as lattice degrees of freedom. The definition of the model is

$$H = -\sum_{\langle \mathbf{i},\mathbf{j}\rangle} t_{\mathbf{ij}}(d_{\mathbf{i}}^{\dagger} d_{\mathbf{j}} + \text{h.c.}) + \sum_{\mathbf{i}} \alpha_{\mathbf{i}} n_{\mathbf{i}} + \sum_{\mathbf{i}} \Delta_{\mathbf{i}} n_{\mathbf{i}}. \qquad (15)$$

This simplified toy model includes a hopping term for spinless fermions (first term), as in the realistic case at large Hund coupling. The hopping amplitude $t_{\mathbf{ij}}$ will first be considered constant and equal to t in this section, but later a random hopping will also be studied for completeness. The most important simplification of Eq. (15), as compared to Eq. (7), is the following: instead of lattice distortions to induce charge ordering, a mere modulation of the chemical potential is introduced "by hand" [the second term in Eq. (15)], where $\alpha_{\mathbf{i}}=+\alpha$ and $-\alpha$ are located on a checkerboard arrangement. This is sufficient to generate the analog of the CO state induced by phonons, namely a charge modulation leading to a checkerboard pattern. In all the toy model simulations reported in this paper α was kept equal to 0.5: for computational simplicity it was not modified to mimic different values of λ and concomitant charge gaps. However, the qualitative results emerging from the analysis are sufficiently clear, that there was no need to further consider α as a tuning variable. Finally, to incorporate the quenched disorder, an on-site random-energy term as in the realistic case was included as well.

The calculation of conductances vs disorder strength, as well as other observables, proceeds straightforwardly for the toy model as a special case of the realistic one. There is no need to carry out any Monte Carlo simulation for the toy model; the results are exact. A remarkable result is shown in Fig. 13, where G vs Δ is shown for both the realistic and the toy models, on the same lattice and at the same temperature. Besides a harmless shift in the location of the peak feature, the shape of the curve is basically the same, revealing insulator-metal-insulator characteristics with increasing Δ in both cases. Then, the simplified toy model is sufficiently robust to have the same properties as the real model, and its analysis will likely unveil the origin of the effect. This is confirmed by a study of the DOS as well (Fig. 14), since the gap in the clean-limit caused by the staggered-modulation in the local-energy induced by the second term of Eq. (15) is filled by the introduction of disorder.

The analysis of the real model—i.e., including phonons and localized spins as active degrees of freedom—was limited to 12×12 lattices and a few realizations of disorder.

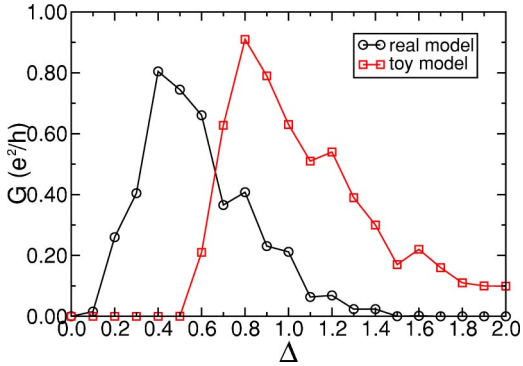

FIG. 13. (Color online) Conductivity vs disorder strength Δ, comparing results for the "real" phononic model, Eq. (7) at $\lambda=0.7$ against the "toy" model. In both cases a bimodal distribution is used, and results are shown using a 12×12 lattice at $T=0.05$. In the calculation of the conductance G for the real model, 10,000 sweeps for thermalization and 2000 for measurements were used. For the toy model the curve shows an average over 100 configurations of disorder, and α is 0.5. The different locations of the conductance peaks can be brought to the same value by modifying α, an unnecessary task in our qualitative study.

With the toy model, a far better study can be conducted. For example, in Fig. 15 an analysis of G vs Δ at several lattices is shown. All of the curves have the same shape, and the size effects are moderate. However, there is a slow decrease in the conductance at the peak. Given the error bars of the simulation (the oscillations in the results between subsequent Δ's can provide a crude estimation of these error bars), and the rapid growth of CPU time with increasing size, an even more careful analysis cannot be carried out. As a consequence, it is not possible in this early investigation to be conclusive about the metallic nature of the state in the bulk 2D limit, particularly in view of the subtleties that are sometimes related with similar studies in the case of Anderson weak-localization effects (this particular issue is quantitatively discussed in the Appendix). Nevertheless, the qualitative analysis to be discussed below will be sufficient to understand the nature of the metallic state in finite-size clusters, as a first step toward applications to real compounds.

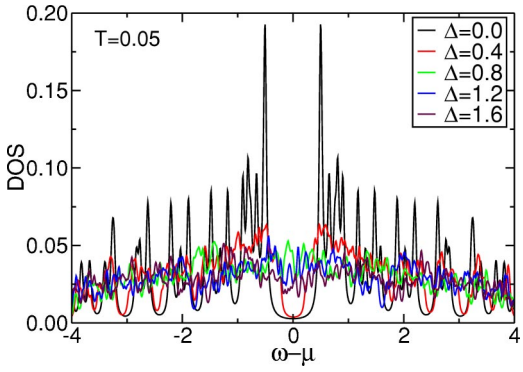

FIG. 14. (Color online) Density-of-states of the toy model, Eq. (15), for several values of the disorder strength Δ. The lattice is 16×16 and temperature $T=0.05$. At the Fermi level states are generated, as it occurs in the realistic model studied in previous sections.

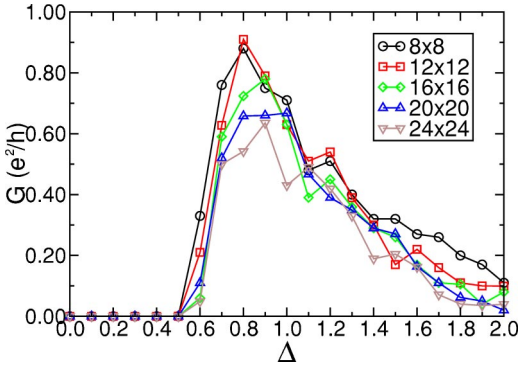

FIG. 15. (Color online) Conductivity vs disorder strength for the toy model, averaged over 100 disorder configurations at $T=0.05$. Results for several cluster sizes are shown. In 2D, conductivity and conductance are the same. The size effects appear to be mild, but the slight reduction of G with lattice sizes in the central region could still lead to an insulating state in the bulk limit. More work is needed to fully understand this subtle issue.

The situation in 3D is similar, since the results for the conductivity (G/L, where the lattice size is L^3) of the toy model seem to converge with increasing size of the cube used for the simulation, as shown in Fig. 16. While it is not impossible that the conductivity could slowly decrease to zero as $L\rightarrow\infty$, the results are suggestive that a metallic state could indeed be found in the bulk 3D limit. More work is needed to fully confirm this assumption.

V. UNDERSTANDING THE METAL-INSULATOR TRANSITION

A. Proposed explanation

The essence to understand the insulator to metal transition found with increasing disorder-strength appears to be very simple, and a starting point is illustrated in Fig. 17. Suppose that in the clean-limit case, $\Delta=0$, the Fermi level is in between two states separated by a gap (and, as a consequence, the state is an insulator). It is natural to expect that with increasing on-site energy disorder those two states will increase their respective widths—since the on-site random en-

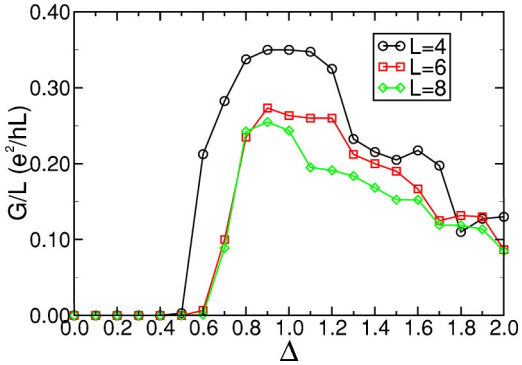

FIG. 16. (Color online) Conductivity (in e^2/hL units) vs disorder strength for the toy model in 3D, averaged over 100 disorder configurations. L is the size length of a L^3 cube.

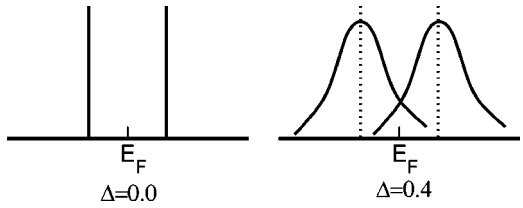

FIG. 17. A cartoonish view of the generation of weight at the Fermi level by disorder. If in the clean limit the system is insulating (with no states available at the Fermi level), the mere broadening of these states by disorder certainly introduces states at E_F after some Δ strength similar to the gap is reached. However, it remains to be investigated whether the states at the Fermi level generated by disorder are truly metallic, or whether they are insulating.

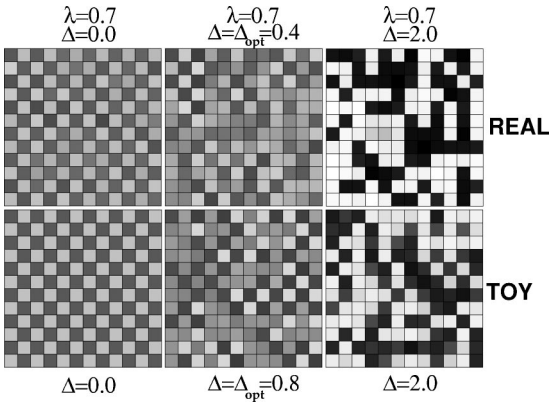

FIG. 18. Monte Carlo "snapshots" obtained using a 12×12 cluster and temperature $T=0.05$ showing the electronic density at each site in tones of black and white. Results are shown for both the "real" and "toy" models [Eqs. (7) and (15), respectively]. In the former, $\lambda=0.7$ is used. In the three cases, results for the clean limit $\Delta=0$, as well as intermediate and large values of Δ are presented. Both the real and toy models at $\Delta=0$ have densities approximately 0.7 and 0.3 in a checkerboard pattern, while at $\Delta=2$ the two clearly-distinguished densities are close to 0.95 and 0.05. A detailed discussion is in the text, but the reader can already visualize the localized nature of the charge in both limits of small and large Δ, while the snapshots at intermediate disorder show a more disordered distribution of populated sites, leading to a metallic state. The similarity between the results for both models is also to be remarked.

ergies directly affect the energy location of the state—and there will be a value of Δ (of the order of the clean-limit gap) where a robust number of states will be located at the Fermi energy. The results we have found in our investigation are compatible with this simple picture for the generation of weight at the Fermi level. In this respect, increasing temperature in the clean-limit at fixed large λ or increasing Δ at fixed small T and large λ appear to be analogous procedures to transform an insulator into a metal. However, Fig. 17 can only be a rough starting point to rationalize the metallic conductance since the presence of states at the Fermi energy is not sufficient to guarantee that the systems is indeed metallic. In fact, Fig. 17 applies even in the limit of vanishing hopping, where the charge is localized.

The most revealing procedure to understand the I-M-I transition with increasing Δ found in the real and toy models involves the study of Monte Carlo "snapshots" of the charge configurations. This is useful in the real model because the classical degrees of freedom freeze at low temperatures, and snapshots are representative of the physics (a state with strong quantum fluctuations may have many configurations with equal weight, complicating the analysis). Typical snapshots are shown in Fig. 18, where results for the electronic density of both the real and toy models are contrasted. It is clear that in the three regimes of relevance—small, intermediate, and large Δ—there is an excellent agreement between the two cases, and the toy model appears to capture the essence of the behavior of the more realistic model, Eq. (7). Let us now analyze the results. At small Δ, the checkerboard pattern certainly prevents the transmission of charge, and the system is insulating in both cases. At large Δ, the sharp color-contrast between the sites occupied and those empty are indicative of a strong localization of charge. Energetically this occurs to take advantage of the regions with large and negative Δ, where at every site either occupancy zero or one is favored. This regime is insulating as well.

The most interesting result occurs at intermediate values of Δ, in the metallic regime. Here the density is closer to its mean value 0.5 in several lattice sites, in spite of the α modulation of the toy model. To understand the results, consider for instance the case of a bimodal distribution for the quenched disorder, as in Fig. 18. Considering the second and third terms of Eq. (15) in the toy model, then locally the effective chemical potential can take four values, namely $\Delta+\alpha$, $\Delta-\alpha$, $-\Delta+\alpha$, or $-\Delta-\alpha$. The case of interest for metallicity is obtained at $\Delta\sim\alpha$ or larger—in excellent agreement with the numerical results—where approximately half the sites have a small effective on-site energy, and these sites are now available for the transport of charge with average density 0.5 [while the other sites either have a very large or very small chemical potential, favoring either minimum (zero) or maximum (one) local occupancy, with both cases not useful for charge transport]. The sites with small effective on-site energy would not contribute to a metal if they were isolated (for instance if they were regularly spaced), but for a *random* distribution of locations a metallic state can be formed if there is a large enough number to induce percolative-like phenomena. Figure 19 further clarifies this issue. The calculations of conductances appear to imply that indeed such percolation has occurred at the densities considered here. This appears to be the essence of the insulator to metal transition. The state that conducts appears to be highly inhomogeneous, compatible with the low value of its conductance. Clearly, insulating regions survive. The elastic cooperative nature of the oxygen coordinates enlarges the regions that are either charge ordered or disordered.

To clarify further the poor nature of the metallic state, a frequently-mentioned issue in the study of conductances is their distribution. Sometimes the mean value, as the one discussed thus far, is not representative due to the large width of the distribution. However, an example of G-distributions is shown in Fig. 20, for the toy model at a value of Δ where G indicates a metallic state. The result shows that the distribution is not abnormally wide, but the only values that visibly appear are 0, 1, and 2, while its full possible range of values

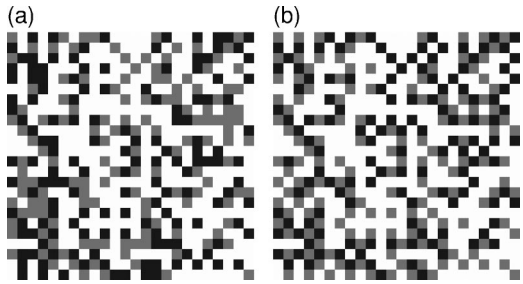

FIG. 19. An example showing that the sites with densities approximately 0.5 are correlated with those with small effective on-site energy, for the particular case $\Delta=0.8$, and $\alpha=0.5$, on a 24 $\times$24 lattice. On the right panel, sites with small effective on-site energy are shown in black if $\Delta-\alpha=0.3$ and light grey if $\Delta-\alpha=-0.3$; the rest are in white. On the left panel, results for the toy model are shown. Here sites with densities between 0.50 and 0.75 are in black, between 0.25 and 0.50 in light grey, and the rest in white. The agreement between left and right is almost perfect. This two-color view helps in the understanding of percolation. In two dimensions the critical percolative fraction is 0.5, precisely the number of sites with small effective on-site energy. The system is then only at the *verge* of percolation. However, in 3D it would be fully percolated since the critical fraction is 0.25.

extends up to 22 in the case of the largest lattice studied. The distribution shown also indicates that slightly less than half the disorder configurations used have zero conductance, while the others have the minimum and next values, borderline compatible with a metal. Then, the metallic state discussed in this paper corresponds to a *poor metal*, and the snapshots previously discussed indicate that this property arises from inhomogeneities. The system appears to be near percolation and, as a consequence, there are only a limited number of paths for conductance across-the-sample.

Although the use of standard formulas for percolative processes could be tempting (for instance to predict the critical density of metallic sites needed to percolate, and the corresponding critical exponents), here the electronic-density at each site is not simply found to correspond to just four numbers, as the effective on-site energies argumentation would indicate. The reason is that the kinetic energy of electrons [the first term in Eq. (15)] must also be considered, and the electronic density "spills" from favorable to unfavorable sites if they are close to one another. This proximity or spilling effect is not considered in traditional models of percolation—where links or sites are sharply either metallic or insulating—preventing the straightforward use of standard formulas deduced for classical random-resistor networks to the case analyzed here.

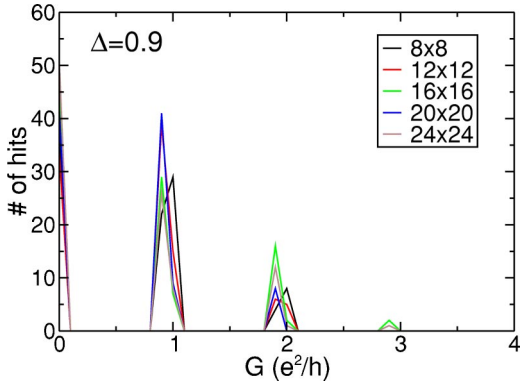

FIG. 20. (Color online) A histogram of conductances observed in the study of the toy model, corresponding to $\Delta=0.9$, and at $T=0.05$, for many values of the disorder. The conductances can only take integer values; here they have been broadened for a better illustration. Size effects appear to be small. Several configurations are insulating ($G=0$), while others conducting (although poorly).

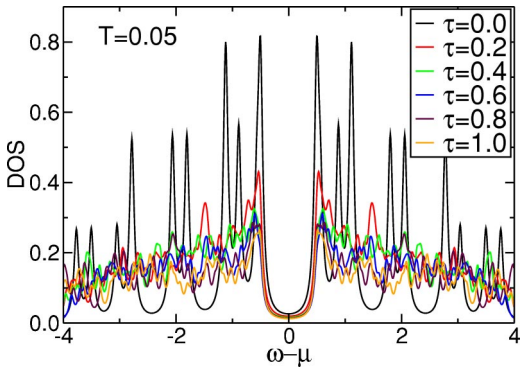

FIG. 21. (Color online) Density-of-states for the toy model where now the disorder is introduced through random hoppings, rather than random on-site energies. Here, the hopping disorder is again a bimodal function with values $\pm\tau$. The results are at $T=0.05$ and obtained on a 12×12 cluster. The gap does not close under the influence of disorder in the hoppings.

B. Consequences of the proposed explanation

1. Results with random hoppings

The model used both here and in the previous investigation[16] employs a local random-energy term as a source of disorder. This form of disorder appears to be crucial for the argumentation discussed in the previous section to explain the stabilization of a poor metallic state at intermediate Δ. The notion of an effective site-energy that nearly cancels at $\Delta\sim\alpha$ for approximately half the sites is very important to render those sites conducting. Then, the present analysis would predict a lack of universality of the disorder-induced insulator-metal transition upon modifications in the explicit form in which the disorder is introduced. In particular, introducing randomness in the *hopping amplitudes*, rather than in the on-site energies, should not lead to a metal according to the previously proposed explanation of the effect, since the effective site energies will not be affected. To verify this idea, in the toy model the on-site disorder was switched off, but now the hopping amplitudes were given an extra random component. More specifically, the hoppings were modified such that $t_{ij}=t+\tau_{ij}$, while Δ_i was switched off in Eq. (15). The random number τ_{ij} was chosen from a bimodal distribution with values $\pm\tau$.

The results for the density-of-states are shown in Fig. 21 for several values of τ. There is a drastic difference when compared with the case of random on-site energies. For random hopping amplitudes the gap present at $\tau=0$ is not filled

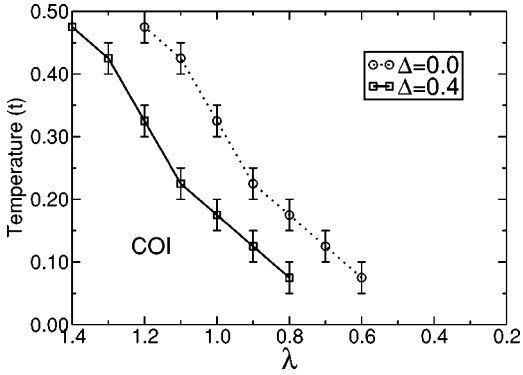

FIG. 22. Phase diagram of model Eq. (7) obtained in the limit where the localized spins are frozen in a ferromagnetic state at all temperatures. As in the case of nonfrozen spins, 10^4 thermalization and 10^4 measurement Monte Carlo sweeps were typically used at each temperature and λ. The lattice was 8×8. The criteria used to determine the transition temperatures are the same as for the simulations with active spins. Results both with and without disorder are shown, with a behavior similar to that found in Fig. 1. The phase diagram at very low temperatures is difficult to obtain due to the rapid increase in CPU time required to remain ergodic (configurations are separated by large energy barriers).

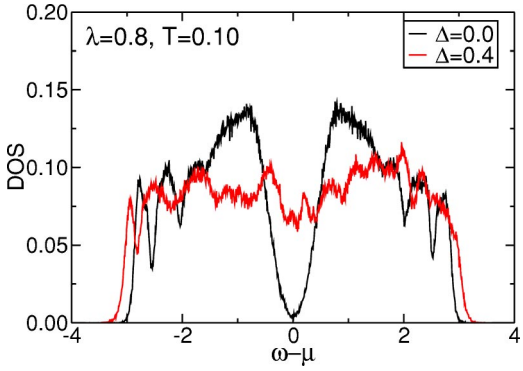

FIG. 23. (Color online) Density-of-states obtained using the model with frozen spins, leaving only the charge as an active degree-of-freedom. The clean-limit gap is still found to close with disorder, even in the absence of CO-FM competition. The lattice is 8×8.

by the random hoppings with increasing τ. The state remains insulating at all values of τ, small, intermediate, and large. This is compatible with the explanation for the insulator-metal transition discussed in the previous subsection, which relies crucially on the effect of on-site disorder.

2. Simulations with frozen spins

Another important prediction of the proposed explanation for the I-M transition is the irrelevancy of the spin degree-of-freedom, and its concomitant FM phase. If the idea is correct, then the presence of the CO vs FM phase competition is not crucial, but more important is the competition between charge-ordered and charge-disordered states. To verify this idea a simulation was carried out, freezing the localized spins to a perfectly ferromagnetic state at all temperatures, effectively removing the spin as a degree-of-freedom. The Monte Carlo phase diagram is shown in Fig. 22 and indeed it shows the expected behavior for the CO state, before and after including disorder.

The density-of-states for the model with only the charge as an active degree-of-freedom is shown in Fig. 23, with and without disorder. The insulator at $\Delta=0$ and metal at $\Delta=0.4$ are present qualitatively as in the case with active spins. It appears that the insulator-metal transition only depends on the presence of charge ordered and disordered states, and their competition. The ferromagnetic component is of no consequence for the effect discussed in this paper.

VI. CONCLUSIONS

In this paper, a simple explanation was proposed for a recently discovered insulator-to-metal transition induced by disorder[16] in a model for manganites with cooperative phonons. The transition occurs when the disorder is introduced in the form of random on-site energies. Our effort presented here confirms the effect, showing that the clean-limit gap in the density-of-states is filled by disorder. Moreover, a calculation of the conductance was implemented, with a Landauer formulation borrowed from the context of mesoscopic physics. This calculation confirms that for intermediate values of the disorder strength Δ the system is indeed metallic, at least for the clusters studied here. A better finite-size scaling should be carried out to fully confirm the metallic nature of the state in the bulk limit, but this huge effort is left for future investigations. Our limited size analysis thus far indicates that the conductivity will remain finite in the bulk limit, particularly in three dimensions.

To understand the origin of this transition, an even simpler model without active phononic degrees-of-freedom was proposed. This new model behaves very similarly as the original one, with a DOS that is filled by disorder, a quite similar conductance vs Δ curve, and similar Monte Carlo snapshots. Both this model and the original one present a percolative-like behavior in the metallic region at intermediate Δ's. The reason is that there are sites where the random energies compensate a dynamically generated on-site energy induced by the interaction with phonons. This interaction produces a checkerboard pattern of charge, leading to sites that are either charge localized $n=1$ (negative effective energy) or empty $n=0$ (positive effective energy). The compensating random energy induces some of the sites to prefer charge $n\sim0.5$, as in a homogeneous metal. It is through these sites that charge can move from one side of the cluster to the other. Compatible with this picture—where only a fraction of the sites have n approximately 0.5—the metallic state is found to have poor-metallic behavior, and in the histogram of conductances for different realizations of quenched disorder many of them have an insulating character. The mechanism here discussed to understand the filling of gaps by disorder appears general, and it should be valid beyond manganites. In fact, there are experimental results and theoretical investigations that have reported similar effects in the context of disordered insulators (see Ref. 22 and references therein). In these related investigations random configurations of disorder were found to provide conducting

resonant electronic channels for tunneling in tunnel junctions, an explanation similar to that provided in the present investigations. In addition, it is known that several materials share phenomenological aspects with the manganites,[23] and the investigations of these interesting effects may have consequences in a variety of research areas.

Is this mechanism active in the real manganites? More work is needed to investigate this issue. Reasons for concern are the dependence of the results with the form of disorder, and the irrelevance of the competing FM state in the process. Disorder in Mn-oxides is believed to arise from lattice distortions induced by chemical doping with ions that are either much larger or smaller than those involved in the parent undoped compound. From this perspective disorder in the hopping amplitudes would be realistic. On the other hand, the ionic dopants have often a different valence than the ion they replaced and that could be represented by on-site energies. Additional effort is needed to relate this simple insulator-metal mechanism to those proposed in early investigations and to experiments. However, even if the immediate relevance of the idea to Mn-oxides needs further study, the effort of Refs. 9 and 16 and ours confirms the key role that disorder plays to render metallic an insulating system, a somewhat counter-intuitive idea. This adds further evidence that the most basic aspects of the original scenario by Burgy *et al.*[7] are essentially correct, namely disorder is needed at least as a triggering effect to induce insulator to metal transitions in models for manganites in the vicinity of regions where FM-AF phase competition occurs. Moreover, the present effort has shown that the metallic state induced by disorder is "poor" due to its inhomogeneous characteristics. All these results provide further support for the mixed-phase-based percolative explanation of the remarkable dc transport behavior of the CMR manganites.

ACKNOWLEDGMENTS

The authors are very thankful to Y. Motome, N. Furukawa, and N. Nagaosa for sharing their ideas about Ref. 16 with us, and for comments on the manuscript. The authors also acknowledge the help of J. A. Vergés in the study of the conductance. The subroutines used in this context were kindly provided by him. The authors are supported by the NSF Grants No. DMR-0122523, No. DMR-0312333, and No. DMR-0303348. Additional funds have been provided by Martech (FSU).

APPENDIX: ISSUES RELATED WITH ANDERSON LOCALIZATION

It is clear in our figures for the conductivity in 2D and 3D, corresponding to the simplified "toy" model, that σ (or the conductance) reaches its maximum value at some intermediate disorder strength $\Delta \sim 0.8-0.9$ (see Figs. 15 and 16). However, both in 2D and 3D the conductance maximum value decreases slowly as the lattice size increases. As discussed in the text, this prevents a clear statement regarding the stability of a metallic phase in the bulk limit by the mechanism discussed in this paper, although the reasons for the metallicity tendencies were properly clarified. The main concern about finding a metal in the bulk is related with issues of Anderson localization, particularly in 2D, as discussed in this appendix.

TABLE I. Differences in conductivities between pairs of lattices in 2D, using data from both the toy model and localization formulas.

L_2	L_1	$\Delta\sigma_{2D}^{toy}(L_1,L_2)$	$\Delta\sigma_{2D}^{loc}(L_1,L2)$
24	20	−0.1167	−0.1161
24	16	−0.1844	−0.2581
24	12	−0.3735	−0.4413
20	16	−0.0677	−0.1421
20	12	−0.2568	−0.3252
16	12	−0.1891	−0.1831

In classical transport theory, which relies on weak scattering, the conductance G of a d-dimensional hypercube of volume L^d is related with the conductivity σ through $G=\sigma L^{d-2}$, where L is much bigger than the mean free path, l. However, Abrahams *et al.* have shown[24,25]—based on renormalization group ideas and perturbation theory—that there is no mobility edge in 2D, hence the conductance should vanish as $L\to\infty$, where quantum interference leads to Anderson localization. According to this picture, the correct scaling of the conductivity in one, two, and three dimensions is given by[25] $\sigma_{1D}(L)=\sigma_0-(2e^2/h)(L-l)$, $\sigma_{2D}(L)=\sigma_0-(2e^2/h\pi)\ln(L/l)$, and $\sigma_{3D}(L)=\sigma_0-(2e^2/h\pi^2)(1/l-1/L)$, respectively, where $\sigma_0=ne^2\tau/m$ is the Drude conductivity at scale l and $\tau=l/\hbar k_F$ is the relaxation time. In 3D, it seems possible to have a nonzero conductance for macroscopic lattice sizes, but not in a lower dimension.

To compare these formulas for localization with our simulations, we proceed as follows. In 2D and 3D, the conductivity attains its maximum value at the disorder strength $\Delta=0.8$ and $\Delta=0.9$, respectively. We define the difference between conductivities for two lattices of sizes L_1 and L_2 as

$$\Delta\sigma_{2D}^{toy}(L_1,L_2)=\sigma_{2D}^{\Delta=0.8}(L_2)-\sigma_{2D}^{\Delta=0.8}(L_1), \tag{A1}$$

$$\Delta\sigma_{3D}^{toy}(L_1,L_2)=\sigma_{3D}^{\Delta=0.9}(L_2)-\sigma_{3D}^{\Delta=0.9}(L_1), \tag{A2}$$

where "toy" indicates that these are the numerical results for the toy model. The corresponding "localization" formulas are given by

$$\Delta\sigma_{2D}^{loc}(L_1,L2)=\frac{2}{\pi}\ln\left(\frac{L_1}{L_2}\right), \tag{A3}$$

$$\Delta\sigma_{3D}^{loc}(L_1,L2)=\frac{2}{\pi^2}\left(\frac{1}{L_2}-\frac{1}{L_1}\right). \tag{A4}$$

In all of the above, the units for conductivity are "e^2/h." The comparison between these formulas is summarized in Table I for the 2D case.

The similarity of the numbers leads to the conclusion that

the numerical results for the 2D toy model in the "metallic regime" could still lead to an Anderson insulator as the lattice size grows. However, obviously the mechanism discussed in this paper is mainly to be applied to 3D manganites (or bilayered systems). It is known that Anderson localization is not so severe in 3D, giving confidence that the state stabilized at intermediate Δ's is indeed a metal in the bulk limit.

[1] *Colossal Magnetoresistance Oxides*, edited by Y. Tokura (Gordon & Breach, New York, 2000); A. Moreo, S. Yunoki, and E. Dagotto, Science **283**, 2034 (1999);Y. Tokura and N. Nagaosa, *ibid.* **288**, 462 (2000).

[2] E. Dagotto, *Nanoscale Phase Separation and Colossal Magnetoresistance* (Springer-Verlag, Berlin, 2002).

[3] M. Uehara, S. Mori, C. H. Chen, and S.-W. Cheong, Nature (London) **399**, 560 (1999); M. Fäth, S. Freisem, A. A. Menovsky, Y. Tomioka, J. Aarts, and J. A. Mydosh, Science **285**, 1540 (1999); Ch. Renner, G. Aeppli, B.-G. Kim, Yeong-Ah Soh, and S.-W. Cheong, Nature (London) **416**, 518 (2002); see also J. W. Lynn, R. W. Erwin, J. A. Borchers, Q. Huang, A. Santoro, J.-L. Peng, and Z. Y. Li, Phys. Rev. Lett. **76**, 4046 (1996), and J. M. De Teresa, M. R. Ibarra, P. A. Algarabel, C. Ritter, C. Marquina, J. Blasco, J. Garca, A. del Moral, Z. Arnold, Nature (London) **386**, 256 (1997); P. G. Radaelli, R. M. Ibberson, D. N. Argyriou, H. Casalta, K. H. Andersen, S.-W. Cheong, and J. F. Mitchell, Phys. Rev. B **63**, 172419 (2001); D. N. Argyriou, J. W. Lynn, R. Osborn, B. Campbell, J. F. Mitchell, U. Ruett, H. N. Bordallo, A. Wildes, and C. D. Ling, Phys. Rev. Lett. **89**, 036401 (2002).

[4] S. Yunoki, J. Hu, A. L. Malvezzi, A. Moreo, N. Furukawa, and E. Dagotto, Phys. Rev. Lett. **80**, 845 (1998); see also E. Dagotto, S. Yunoki, A. L. Malvezzi, A. Moreo, J. Hu, S. Capponi, D. Poilblanc, and N. Furukawa, Phys. Rev. B **58**, 6414 (1998); S. Yunoki, A. Moreo, and E. Dagotto, Phys. Rev. Lett. **81**, 5612 (1998); A. Moreo, S. Yunoki, and E. Dagotto, *ibid.* **83**, 2773 (1999).

[5] E. Dagotto, T. Hotta, and A. Moreo, Phys. Rep. **344**, 1 (2001).

[6] S. H. Pan, J. P. O'Neal, R. L. Badzey, C. Chamon, H. Ding, J. R. Engelbrecht, Z. Wang, H. Eisaki, S. Uchida, A. K. Gupta, K.-W. Ng, E. W. Hudson, K. M. Lang, and J. C. Davis, Nature (London) **413**, 282 (2001); see also J. M. Tranquada, B. J. Sternlieb, J. D. Axe, Y. Nakamura, and S. Uchida, *ibid.* **375**, 561 (1995).

[7] J. Burgy, M. Mayr, V. Martin-Mayor, A. Moreo, and E. Dagotto, Phys. Rev. Lett. **87**, 277202 (2001); see also A. Moreo, M. Mayr, A. Feiguin, S. Yunoki, and E. Dagotto, *ibid.* **84**, 5568 (2000); M. Mayr, A. Moreo, Jose A. Verges, J. Arispe, A. Feiguin, and E. Dagotto, *ibid.* **86**, 135 (2001).

[8] D. Akahoshi, M. Uchida, Y. Tomioka, T. Arima, Y. Matsui, and Y. Tokura, Phys. Rev. Lett. **90**, 177203 (2003).

[9] H. Aliaga, D. Magnoux, A. Moreo, D. Poilblanc, S. Yunoki, and E. Dagotto, Phys. Rev. B **68**, 104405 (2003).

[10] T. J. Sato, J. W. Lynn, and B. Dabrowski, *Disorder-Induced Polaron Formation in the Magnetoresistive Perovskite* $La_{0.54}Ba_{0.46}MnO_3$, preprint.

[11] J. Burgy, A. Moreo, and E. Dagotto, Phys. Rev. Lett. **92**, 097202 (2004).

[12] Y. Imry and S. K. Ma, Phys. Rev. Lett. **35**, 1399 (1975); see also J. F. Fernandez, G. Grinstein, Y. Imry, and S. Kirkpatrick, *ibid.* **51**, 203 (1983).

[13] The potential importance of elastic effects has been remarked by D. I. Khomskii and K. I. Kugel, Europhys. Lett. **55**, 208 (2001); Phys. Rev. B **67**, 134401 (2003). See also A. R. Bishop, T. Lookman, A. Saxena, and S. R. Shenoy, Europhys. Lett. **63**, 289 (2003); J-X. Zhu, K. H. Ahn, Z. Nussinov, T. Lookman, A. V. Balatsky, and A. R. Bishop, Phys. Rev. Lett. **91**, 057004 (2003); see also T. Lookman, S. R. Shenoy, K. Ø. Rasmussen, A. Saxena, and A. R. Bishop, Phys. Rev. B **67**, 024114 (2003); K. H. Ahn, T. Lookman, A. Saxena, and A. R. Bishop, cond-mat/0207224; A. Bussmann-Holder and A. R. Bishop, Phys. Rev. B **56**, 5297 (1997). See also S. Semenovskaya and A. G. Khachaturyan, Phys. Rev. Lett. **67**, 2223 (1991); M. J. Calderón, A. J. Millis, and K. H. Ahn, cond-mat/0305440; K. H. Ahn and A. J. Millis, Phys. Rev. B **64**, 115103 (2001).

[14] K. Yang, Phys. Rev. B **67**, 092201 (2003).

[15] See for instance, J. Burgy, E. Dagotto, and M. Mayr, Phys. Rev. B **67**, 014410 (2003); and D. Khomskii and L. Khomskii, *ibid.* **67**, 052406 (2003).

[16] Y. Motome, N. Furukawa, and N. Nagaosa, Phys. Rev. Lett. **91**, 167204 (2003).

[17] T. Hotta, S. Yunoki, M. Mayr, and E. Dagotto, Phys. Rev. B **60**, R15 009 (1999); S. Yunoki, T. Hotta, and E. Dagotto, Phys. Rev. Lett. **84**, 3714 (2000); T. Hotta, A. Feiguin, and E. Dagotto, *ibid.* **86**, 4922 (2001); T. Hotta, M. Moraghebi, A. Feiguin, A. Moreo, S. Yunoki, and E. Dagotto, *ibid.* **90**, 247203 (2003). See also S. Yunoki, T. Hotta, and E. Dagotto, Phys. Rev. Lett. **84**, 3714 (2000).

[18] J. A. Vergés, V. Martín-Mayor, and L. Brey, Phys. Rev. Lett. **88**, 136401 (2002).

[19] The use of, e.g., $\langle n_{\mathbf{i}}\rangle\langle n_{\mathbf{i+x}}\rangle$ instead of $\langle n_{\mathbf{i}}n_{\mathbf{i+x}}\rangle$ is merely for technical convenience, and at low temperatures it does not affect our main conclusions.

[20] J. A. Vergés, Comput. Phys. Commun. **118**, 71 (1999).

[21] E. Dagotto, Rev. Mod. Phys. **66**, 763 (1994).

[22] E. Yu. Tsymbal, and D. G. Pettifor, Phys. Rev. B **58**, 432 (1998); and references therein.

[23] H. Rho, C. S. Snow, S. L. Cooper, Z. Fisk, A. Comment, and J. Ph Ansermet, Phys. Rev. Lett. **88**, 127401 (2002); C. S. Snow, S. L. Cooper, G. Cao, J. E. Crow, H. Fukazawa, S. Nakatsuji, and Y. Maeno, *ibid.* **89**, 226401 (2002); G. Alvarez, M. Mayr, and E. Dagotto, *ibid.* **89**, 277202 (2002); M. Mayr, G. Alvarez, and E. Dagotto, Phys. Rev. B **65**, 241202(R) (2002); G. Alvarez and E. Dagotto, *ibid.* **68**, 045202 (2003).

[24] E. Abrahams, P. W. Anderson, D. C. Licciardello, and T. V. Ramakrishnan, Phys. Rev. Lett. **42**, 673 (1979).

[25] P. A. Lee, and T. V. Ramakrishnan, Rev. Mod. Phys. **57**, 287 (1985).